decay-energy release at shutdown is approximately 6.5 Mw and at the end of 66.8 hr, 8 kw. To conserve hydrogen, the decay heat is absorbed primarily by discrete mass-flow pulses operating within a 100°R temperature band. However, some continuous flow of hydrogen at low-mass flow rates is used to keep the reactor structural support elements from overheating during the early part of pulse cooldown. Later, this continuous flow is terminated, and there will be long periods of zero-flow plus discrete pulses of flow. In Fig. 10, the small continuous flow is 0.40 lb/sec (thrust = 190 lbf) from start of cooldown to the seventh pulse which occurs 0.44 hr later. The large pulses, which are superimposed on top of the continuous flow, have a total of 1.7 lb/sec flow rate (thrust = 790 lbf) until the seventh pulse, after which it is changed to 0.70 lb/sec. The pulse frequency is very low at the end of cooldown, as illustrated. This pattern of pulses can be varied considerably by changing maximum and minimum temperature limits and, therefore, should be considered as only illustrative.

The impulse characteristics of cooldown are illustrated in Fig. 11 for Burn No. 1, which was discussed above. This shows the effect of the rapid rate of energy release during the very early stages of cooldown relative to the later times. The total impulse during this cooldown amounts to 2.8 million lb/sec (or 2.35% of the total impulse of Burn No. 1). The maximum ideal velocity increment is 380 fps. Most of the cooldown impulse (90%) is realized in the first 20 hr of cooldown operation. The cooldown impulse is considered as part of the useful impulse, and in the above case (leave-Earth burn), it can be considered to be similar to an extended velocity trim system that that could be useful for trajectory correction purposes. After other burns, when approaching Earth or lunar rendezvous orbit, it can be used to gradually trim into the desired orbital position. The nuclear shuttle is assumed to have a chemical reaction control system that will be used for precise rendezvous and docking maneuvers.

## Summary

Various potential missions are being studied to determine NERVA engine requirements; one of the most demanding is the Earth-lunar reusable-nuclear-shuttle, eight-burn mission. Ultimately, the reusable nuclear shuttle may be serviced and supplied by a low-cost, Earth-to-orbit, reusable chemical shuttle; but for design purposes, it is presently assumed that Saturn launch vehicles and Saturn derivative nuclear stages will be used. However, the long-range objective of low cost is influential in reaching current design decisions, as illustrated in the selection of an engine throttling mode. Other characteristics of the engine design are a specific impulse of 825 sec at a thrust level of 75,000 lb; a 10-hr lifetime with up to 60 restarts; restart capability at any time; zero-NPSP dual pumps for supply-tank pressures of 15 to 30 psia; capability of supplying tank pressurization gas; high-accuracy controls; thrust-vector control; man-rating; 0.995 reliability; five-year ground and three-year space storability; propellant-feed-system malfunction mode; emergency abort mode for flight safety; and space maintenance of critical items.

## References

[1] Prepared testimony presented to the Subcommittee on Advance Research and Technology, Committee on Science and Astronautics, the U. S. House of Representatives, Feb. 25, 1970.

[2] Buden, D., "Operational Characteristics of Nuclear Rockets," *Journal of Spacecraft and Rockets*, Vol. 7, No. 7, July 1970, pp. 832–836.

[3] Durkee, W. E. and Damerval, F. B., "Nuclear Rocket Experimental Engine Test Results," AIAA Paper 70-709, San Diego, Calif. 1970; also *Journal of Spacecraft and Rockets*, Vol. 7, No. 12, Dec. 1970, pp. 1397–1402.

JULY 1971 J. SPACECRAFT VOL. 8, NO. 7

# An Active Radiation Shield for Cylindrically Shaped Vehicles

S. H. Levine* and R. Lepper†
*Northrop Corporate Laboratories, Hawthorne, Calif.*

**An effective magnetic shield design has been developed for protecting a cylindrical space vehicle from space electron radiation. It employs a few coils of equal diameter (and approximately twice the vehicle diameter) located coaxially about the vehicle. The magnetic shield simulator (MAGSIM) has been used to develop engineering data for designing this shield. The data are presented nondimensionally and can be used to design a cylindrical shield of any size; as an example, an active shield for a 10-ft-diam, 30-ft-long vehicle is designed, assuming a current density in the superconductor of $2.5 \times 10^5$ amp/cm$^2$ at 10°K. This shield protects against electrons with a 7-Mev cutoff energy, produces ~500 gauss inside the vehicle, and weighs 525 lb.**

## Introduction

A MAJOR hazard of manned space travel is radiation damage to both the crew and some electronic components of the vehicle. For many Earth-orbit missions, the principal radiation hazard is that of the natural and artificial radiation belts composed of trapped relativistic electrons and high-energy protons. Because of the tremendous weight penalty imposed by passive material shields and the potential weight savings afforded by active electromagnetic shields, numerous studies of active shields have been made, with promising results.[1-3] Their advantage over material shields is greatest when the radiation hazard is limited to the relativistic electrons. The relatively low mass of the electron makes it easy for moderately intense magnetic fields to deflect electrons away from the vehicle, and thus the hazardous bremsstrahlung radiation that is produced in any material shield (and requires additional massive shielding) is precluded in active

Received July 16, 1970; revision received March 18, 1971. This program has been supported by the Air Force Avionics Laboratory under Contract AF 33(615)3831, Leo Krautman, project monitor.

* Acting Director, Electromagnetics Laboratory; now Director, Nuclear Reactor Facility, The Pennsylvania State University, University Park, Pa. Member AIAA.

† Senior Engineer, Member of the Technical Staff, Materials Sciences Laboratory. Member AIAA.

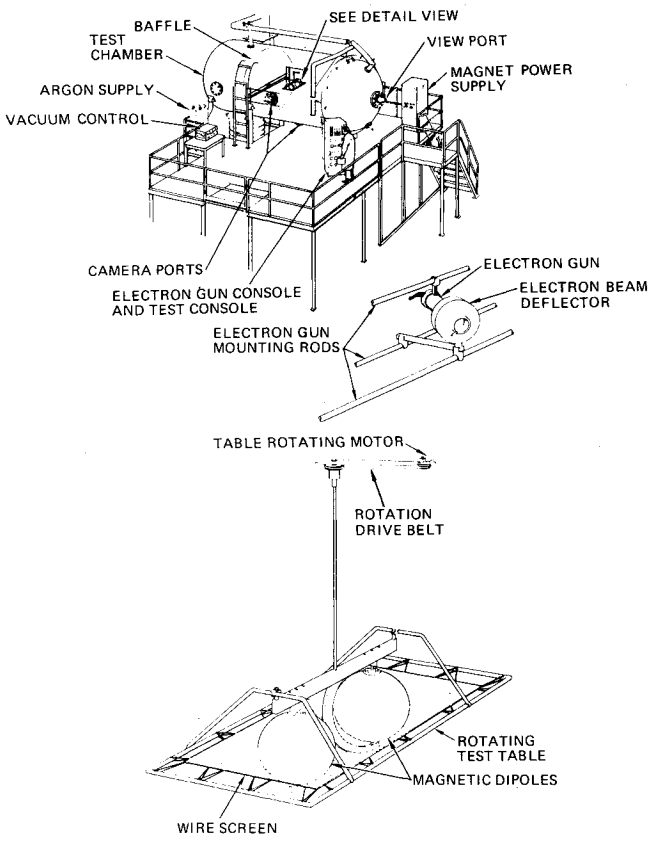


**Fig. 1 The magnetic shield simulator MAGSIM.**

shields. However, the active shield is not without its problems, including shaping of the protective region to match the shape of the vehicle (or vice versa). Since the divergence characteristics of the magnetic field always produce toroidally-shaped protected or forbidden regions, active shield designs, to date, have been limited to toroidal vehicles. On the other hand, almost all U.S. space vehicles designed for the next decade are principally cylindrical. For this reason the magnetic shield simulator (MAGSIM)[3-5] has been used to design an active shield for cylindrical vehicles.

The MAGSIM is, essentially, an analogue device, which utilizes the Stormertron principle[6] for scaling charged-particle orbits in externally-deflecting magnetic fields. It was developed to measure the protected regions produced by active shields of complex shapes. Figure 1 shows its arrangement with two point dipole magnets suspended in the screen grid. The wires of the grid are coated with fluorescent material, so that the impenetrable or dark regions about the magnet in the plane of the grid are clearly outlined by the electron excitation of the wire.

This paper presents a) the techniques for taking and depicting the data in nondimensional parameters and b) an example design of an active shield for a 10-ft-diam × 30-ft-long cylindrical vehicle.

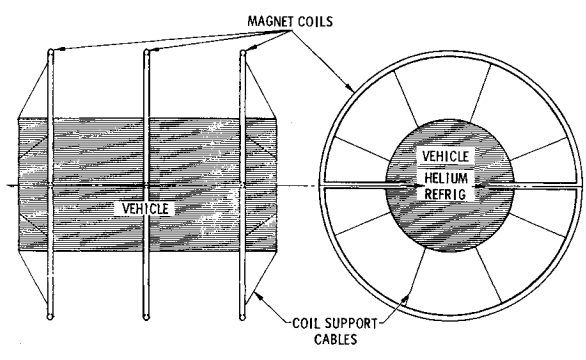


**Fig. 2 Schematic of magnetic shield for cylindrical vehicle.**

## MAGSIM Data and Shield Design

The optimum active shield configuration found to date is shown in Fig. 2. Individual coils are mounted parallel to, and coaxial with, the vehicle. The MAGSIM has been used to establish the size and spacing of the coils by providing an outline of the dark protected region as shown in Fig. 3. The ends of the cylinder are not protected by this design; however, practical designs for present space vehicles have equipment compartments at both ends which provide natural material shields for the central living and experiment quarters. It also should be noted that, in general, electrons spiral about the Earth's magnetic field providing an anisotropic source distribution similar to that of protons.[7,8] Such electron motion, combined with forced space orientation of the vehicle, has been shown by MAGSIM data[9] to provide partially-protective regions at both ends of the cylinder for this shield configuration.

Relatively low currents are used in the coils to produce the protected region shown in Fig. 3. Note that in this case there is a slight bowing out of the protective shape so that the radius in between the coils, $r_m$, is greater than that adjacent to the coils, $r_v$. At even lower currents in the coil, the shape of the protective regions bows inward making $r_v > r_m$. In this latter case, if the current in the coils is increased, a condition is reached wherein the protected region becomes that of a perfect cylinder, i.e., $r_v = r_m$. Long cylinders will require more than two coils; consequently, a three-coil configuration was built and tested, and the third coil extended the protective region as expected.

It may be noted that the dark or protected area is not symmetrical with respect to the axis through the coils. The minimum or smaller area is always attained on the side opposite the electron source, consistent with previous MAGSIM data. A cylindrical volume having the cross section of the outline of the smallest symmetrical protected region is the protective region. Thus, the minimum forbidden volume is symmetrical about the coil axis forming a spool-type shape. The cylinder representing the shape of the space vehicle, scaled down to the size of the MAGSIM apparatus, is represented by a radius $r_0$ and must be totally enclosed within the spool-type shape. Because of the bowing the protective volume is greater than that of the vehicle except for one coil current.

Two scaling factors, $L$ and $G$, are now defined:

$$L = r_0/a_1 = R_0/a, \qquad G = d_1/a_1 = d/a \tag{1}$$

where $r_0$ and $R_0$ are radii of forbidden volumes used in MAGSIM and on the space vehicle, $a_1$ and $a$ are wheel radii of the coils used in MAGSIM and on the space vehicle, and $d_1$ and $d$ are the lengths of the forbidden volumes between pairs of coils used in the two cases.

Values of $L$ and $G$ from the MAGSIM data are plotted in Figs. 4 and 5, respectively. The solid curves of Fig. 4 present $L$ vs coil current $i$ for several values of $G$ which can be used directly in the design calculations. The dashed curves show the bowing-out effect in Fig. 3 where $r_m > r_v$, and the solid curves refer to the minimum radius for all data. The data in Figs. 4 and 5 were taken using a pair of identical coils having a wheel radius $a_1 = 4.125$ in. and spaced 4, 5.125, 8, and 10 in. apart. These data were taken with the ends of the coils blocked to simulate spacecraft shielding, and the minimum volumes were obtained by varying the orientation of the vehicle relative to the electron gun.

For scaling $a_1$ and the coil current $i$, the parameter

$$\lambda = a_1/C_{st_1} = a/C_{st} \tag{2}$$

is used, where the Stormer radius[10,11] $C_{st}$ is

$$C_{st} = (qM/pc)^{1/2} \quad (3)$$

The subscript 1 refers to the MAGSIM parameters; otherwise, the parameters relate to the actual space vehicle and the electron radiation in space. In Eq. (3), $q$ is the particle charge (for an electron $q = 4.8 \times 10^{-10}$ esu), $c$ is the velocity of light ($3 \times 10^{10}$ cm/sec), $p$ is the momentum of the particle, and $M$ is the magnetic moment of the coil ($\pi Ia^2/10$, where $I$ is in amp-turns). Substitution of the values of the MAGSIM parameters in Eq. (3) yields

$$\lambda = 3.28(V/I^2)^{1/4} \quad (4)$$

where $V$ is the electron gun accelerating voltage (350 v) and $I = 615\ i$, the 615 referring to the number of turns in each coil. Thus, with these values, Eq. (4) further reduces to

$$\lambda = 0.571(i)^{-1/2} \quad (5)$$

which permits a determination of $\lambda$ directly from the coil current.

We will assume a maximum electron energy of 7 Mev (cutoff energy) for the space electron environment. The trapped electron energy spectrum falls off extremely fast above a few Mev, so that the contribution to the spectrum above 7 Mev can be neglected. This approximation is particularly valid here since the active shield continues to provide partial shielding for electrons with energies above 7 Mev. Using the momentum of 7-Mev electrons ($3.74 \times 10^{-16}$ g-cm/sec) in Eq. (2), we obtain the relation for the corresponding ampere-turns in the space vehicle coils, i.e.,

$$I = 7.41 \times 10^4 \lambda^{-2} \quad (6)$$

Let us use Eqs. (5) and (6) to design an active shield for a 10-ft-diam, 30-ft-long space vehicle. Three coils spaced 15 ft apart are required. The various parameters have been calculated for several coil radii (Table 1). The data in Table 1 are used to compute the mass of the magnetic shield system,

$$M_T = M_m + M_{cry} + M_{pc} \quad (7)$$

where $M_m$ = mass of the magnet (3 coils), $M_{cry}$ = mass of the cryogenic cooling system, and $M_{pc}$ = mass of the ancillary support equipment. We shall determine the masses of these three principal subsystems for one coil radius, $a = 10$ ft (20-ft diam). The other coil radii listed in Table 1 produce somewhat greater masses of the total system.

### Mass of the Magnet

The mass of the magnet comprises the masses of the magnet superconductor ($M_c$), the surrounding helically wound copper spacer ($M_{ss}$), a titanium tube for piping the helium coolant around the superconductor ($M_{st}$), and coil support cables ($M_{sc}$):

$$M_m = M_c + M_{ss} + M_{st} + M_{sc} \quad (8)$$

The copper spacer positions the superconductor in the center of the titanium tube to permit unrestricted flow of the helium coolant around the superconductor. The spacing between the superconductor is chosen to be 0.200 cm; consequently, the diameter of the helical copper spacer is 0.200 cm. For the three coils, it can readily be shown that

$$M_{ss} = 5.16 \times 10^{-2}\, a(\text{lb}) \quad (9)$$

**Table 1 Data for three parallel coils**

| $a$, ft | $L$ | $G$ | $i$, amp | $\lambda$ | $I$, amp turn |
|---|---|---|---|---|---|
| 9 | 0.556 | 1.666 | 1.170 | 0.528 | $2.80 \times 10^5$ |
| 10 | 0.500 | 1.500 | 0.895 | 0.604 | $2.14 \times 10^5$ |
| 12 | 0.417 | 1.250 | 0.650 | 0.706 | $1.57 \times 10^5$ |
| 14 | 0.357 | 1.071 | 0.490 | 0.816 | $1.17 \times 10^5$ |

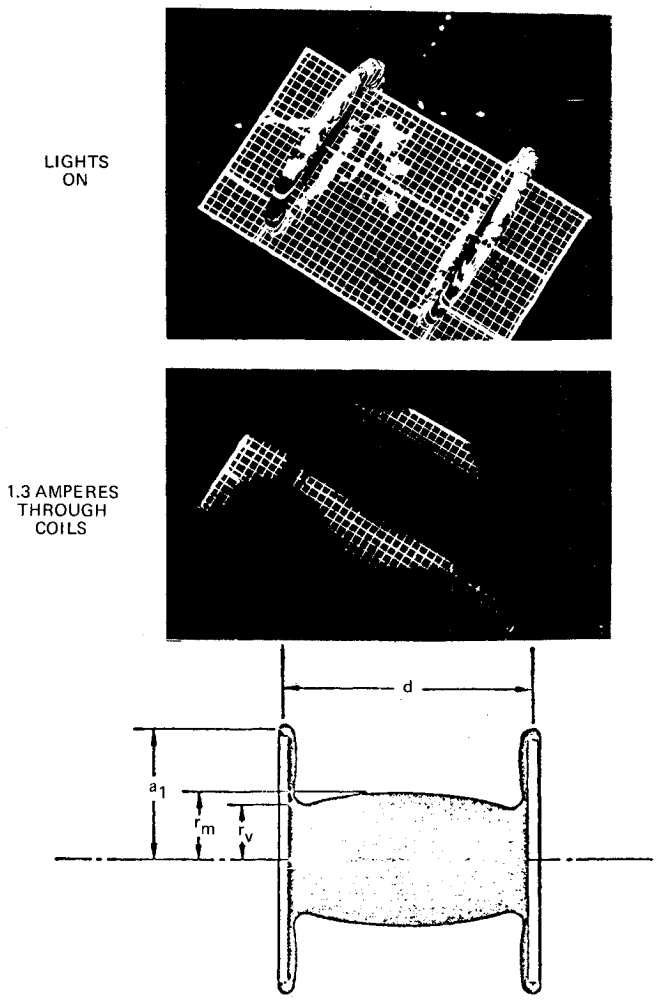


**Fig. 3 Forbidden area in meridian plane of two-coil configuration.**

Letting $R_1$ and $R_2$ be the inner and outer radii of the titanium tube,

$$M_{st} = \rho_{Ti}\pi^2(R_2^2 - R_1^2)\cdot 6a \quad (10)$$

where $\rho_{Ti}$ = density of titanium, and $R_2 = R_1 + 0.076$ cm.

Standard stress calculations, which account for the magnetic field-coil current interactions, show that a $\frac{1}{16}$-in.-diam, flexible, corrosion-resisting, stainless-steel aircraft cable can withstand the load on the end coils; this cable has an allowable load of 480 lb and weighs 0.75 lb/100 ft. Therefore, the mass for all three loops is $M_{sc} = 6$ lb.

The mass of the conductor is inversely related to the cur-

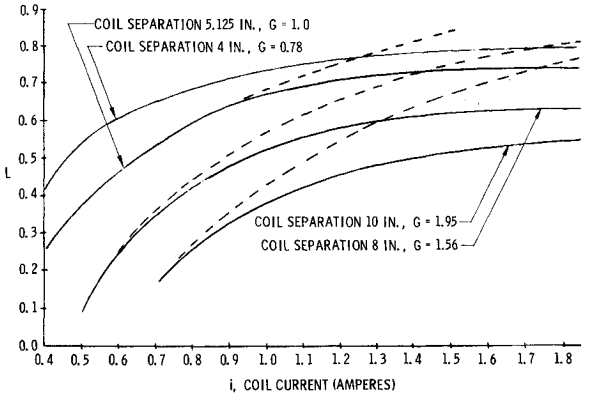


**Fig. 4 $L$ (forbidden volume radius/coil radius) vs coil current $i$ for several values of $G$ (forbidden zone between coils/coil radius).**

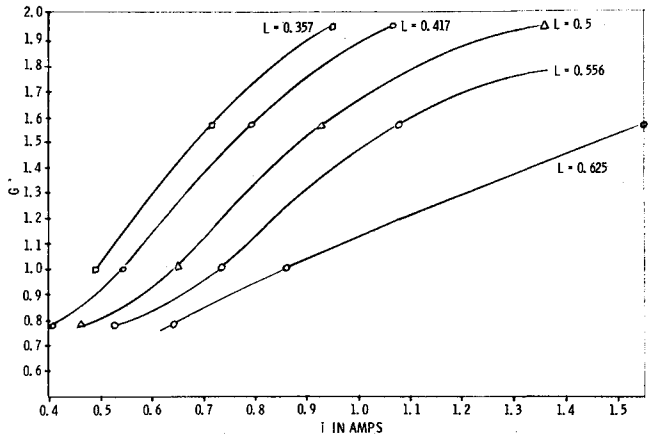


**Fig. 5 $G$ vs $i$ for several values of $L$.**

rent density $j$:

$$M_c = 6\pi\rho_d a/jf_p \tag{11}$$

where $\rho_d$ is the density of the superconductor wire and $f_p$ is the packing fraction of the coil. We assume that a coil can be constructed which attains $j = 2.5 \times 10^5$ amp/cm$^2$ at a temperature $T$ of 10°K. Special manufacturing procedures and special studies regarding quality control will probably be necessary before such conditions can be attained. Current densities measured with small-diameter, $Nb_3Zr$ wires by Betterton et al.,[12] have been $1 \times 10^6$ amp/cm$^2$ in a 4000-gauss field and $1.8 \times 10^6$ amp/cm$^2$ in a zero-gauss field at 4.2°K. Higher $j$'s have been found with $Nb_3Sn$ conductors. For 4.2°K $\leq$ 14°K, the critical current for $Nb_3Sn$ superconductors can be expressed:[13]

$$j = j_0(1.3 - T/14) \tag{12}$$

where $j_0$ is the current density at 4.2°K. It should be possible to attain an effective current density in $Nb_3Sn$ coils of $2.5 \times 10^5$ amp/cm$^2$ ($j_0 = 4.3 \times 10^5$ amp/cm$^2$) at 10°K. A dependence on the higher powers of $(T/T_c)$ in Eq. (12) would only make the present estimates relatively more conservative. Using Eqs. (8–11), $M_m$ is found to be 125 lb for the 10-ft-diam coil, of which $M_c = 87$ lb ($R_0 = 0.520$ cm) using $f_p = 1$. Calculations also showed that the coil could withstand the self-induced hoop stress.

### Mass of the Cryogenic Cooling System

We can subdivide $M_{cry}$ into the mass of the insulation $M_I$, the mass of the refrigerator $M_R$, the incremental mass of the power supply $M_p$, and the mass of the radiator, $M_{rad}$:

$$M_{cry} = M_I + M_R + M_p + M_{rad} \tag{13}$$

where $M_I = 6\pi^2 a(R_3^2 - R_2^2)\rho_I$, where $R_3$ and $R_2$ are the outside and inside radii of the superinsulation wrapped around the titanium coolant tube, and $\rho_I$ is the density of the superinsulation (1 lb/ft$^3$ for Dimplar material). The heat leakage into the helium coolant, $Q$, can be expressed as

$$Q = 2\pi K_e \Delta T_1 L_1/\ln R_3/R_2 \tag{14}$$

where $K_e$ = effective thermal conductivity, $L_1$ = total length of insulation, and $\Delta T_1 = T_1 - T_0$ = temperature drop across insulation, where $T_0$ = superconductor wire temperature, and $T_1$ = average temperature on outer surface of insulation. Considering the effects of sunlight, earth albedo, space vacuum, and thermal radiation from the vehicle external skin on the outer insulation layer for the magnet coils, it turns out that $T_1 = 200$°K (360°R). Using $R_3/R_2 = 7$, the heat leakage per foot at $T_0 = 10$°K is $Q/L_1 = 0.018$ w/ft, and $M_I = 20$ lb.

We obtain $M_R$ and the power requirements from the curves presented in Fig. 6. These curves are considered near state-of-the-art and represent anticipated power and weight requirements for a refrigerator based on Arthur D. Little's[14] design criteria for a 1-$w$, 3.6°K, 100-lb, rotary-stroking refrigerator. (This rotary refrigerator is, itself, designed for satellite purposes). To use the curves of Fig. 6, it is necessary to establish the power requirement from Eq. (14). For the 10-ft-diam coils, the design requires a $Q$ of 3.3, and consequently $M_R = 82$ lb, and the power requirement for the refrigerator system is 1.05 kw. Using the conversion factor 0.1 lb/w,[14] $M_p = 105$ lb. We assume that the raditor mass is 0.12 $M_p$, in accordance with A. D. Little's findings[14]; consequently, $M_{rad} = 13$ lb and $M_{cry} = 220$ lb.

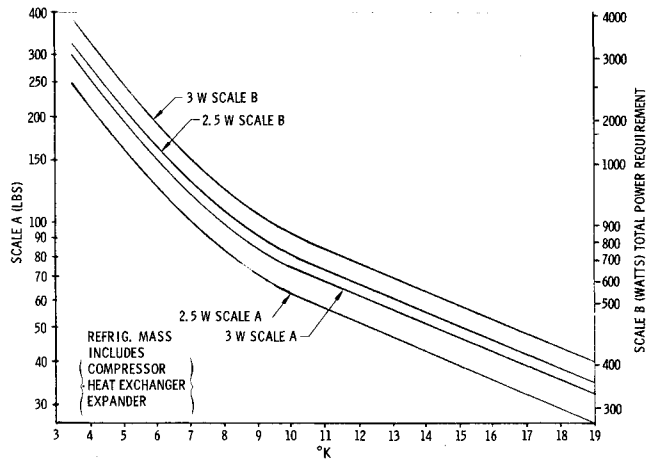


**Fig. 6 Refrigerator mass and power requirements data curves (5 yr state-of-the-art).**

### Total System Mass

We will assume that the power conditioning equipment, start-up power supply for energizing the superconductor, and miscellaneous items that will have to be added to the system to integrate the magnet system into the spacecraft, increase the mass of the system by approximately another 50%. Thus,

$$M_{pc} = 0.5(M_m + M_{cry}) \tag{15}$$

and

$$M_T = 1.50(M_m + M_{cry}) \tag{16}$$

Using Eq. (16) and the component masses, $M_T = 525$ lb.

## Conclusion

Despite the characteristic toroidal protective regions generated by the magnetic fields, the MAGSIM has been effectively and efficiently utilized to determine a shield configuration for protecting cylindrical vehicles. The total shield mass of 525 lb—required to protect the large size vehicle considered from relativistic electrons—is relatively low, particularly compared with the mass of an aluminum shield surrounding only the cylindrical section of the vehicle. A 4.5-ton aluminum shield, of the configuration stated, is required just to stop 7-Mev electrons, and this does not include any shielding of the resulting bremsstrahlung radiation. Thus, for protection against space electron radiation, the active shield promises excellent weight advantages over material shields.

Calculations have been also performed to determine the mass of these shields for the other coil radii listed in Table 1; however, the 10-ft radius is close to the optimum size for the 10-ft-diam vehicle. The 30-ft length, however, is not the optimum length for spacing the three magnets on the space vehicle, but two magnets by themselves will not suffice to protect the full length of the vehicle.

The optimum temperature of the superconductor coil is near 10°K; at higher operating temperatures, the current density begins to drop, causing the mass of the magnet and insulation to increase more than the mass of the radiator and power supply decreases; at lower temperatures, the opposite trends occur.

A digital computer program has been used to determine the magnetic field intensity inside the space vehicle. The maximum allowable value probably is of the order of 500 gauss; higher values affect the operation of standard relays and many other devices. Increasing the radius of the coils will reduce the magnetic fields inside the vehicle at some cost in shielding mass. It may be more advantageous to incorporate special shielded regions inside the space ship for housing the sensitive components. It should also be mentioned that future advances in super-conductivity and low-temperature cooling systems will greatly benefit active shields, whereas no avenue for significant improvement in material shields is foreseen.

## References


[1] Levy, R. H., "Radiation Shielding of Space Vehicles by Means of Superconducting Coils," *ARS Journal*, Vol. 31, 1961, p. 1568.

[2] Bhattacharjie, A. and Michael, I., "Mass and Magnetic Dipole Shielding Against Electrons of the Artificial Radiation Belt," *AIAA Journal*, Vol. 2, No. 12, Dec. 1964, pp. 2198–2201.

[3] Levine, S. H. and Lepper, R., "Analogue Studies of Magnetic Shields," *AIAA Journal*, Vol. 6, No. 4, April 1968, pp. 695–701.

[4] Levine, S. H. and Lepper, R., "Magnetic Shield Simulator," *Annual Technical Proceedings*, Institute Environmental Sciences, 1965.

[5] Levine, S. H., Bhattacharjie, A., and Lepper, R., "Forbidden Regions Produced by Two Parallel Dipoles," *AIAA Journal*, Vol. 4, No. 4, April 1966, p. 654–658.

[6] Stormer, C., Chapter II, *The Polar Aurora*, Oxford University Press, New York, 1955, p. 229.

[7] Vette, J. I., "Models of the Trapped Radiation Environment," Vol. I, *Inner Zone Protons and Electrons*, and Vol. II, *Inner and Outer Zone Electrons*, NASA SP-3024, 1966.

[8] Fortney, R. E. and Duckworth, G. D., "The Importance of Radiation Anisotropy in Dose Calculations," *Second Symposium on Protection Against Radiation in Space*, NASA SP-71,1964.

[9] Levine, S. H. and Lepper, R., "Analogue Studies of Active Radiation Shielding," AFFDL-TR-67-66, June 1967, Air Force Flight Dynamics Lab.

[10] Janossy, L., Chapter VII, *Cosmic Rays*, Oxford at the Clarendon Press, 1950, p. 270.

[11] Montgomery, D. J. X., *Cosmic Ray Physics*, Princeton University Press, Princeton, N.J., 1949, p. 316.

[12] Betterton, J. O. et al., *Superconductors*, Interscience, New York, 1962.

[13] Foner, S., Private Communication, National Magnet Lab., MIT, May 1968.

[14] Little, A. D., "Exploratory Development of a 3.6°K Rotary Stroking Refrigerator," RTDPRNR. 20534, April 14, 1966.


JULY 1971 J. SPACECRAFT VOL. 8, NO. 7

# Accelerometer Calibration in the Low-$g$ Range by Means of Mass Attraction


KONRAD REINEL*

*Deutsche Forschungs- und Versuchsanstalt fuer Luft- und Raumfahrt e.V., Oberpfaffenhofen, Germany*



**Mass attraction is used as an acceleration input to calibrate an accelerometer. The upper limit of the acceleration by a reasonable mass size is $10^{-9}$ $g$ in orbit and $10^{-7}$ $g$ in the laboratory. The calibration has been carried out in the laboratory for an electrostatic suspended single-axis accelerometer (MESA) with a variable mass attraction. The tilting of the test pad was avoided by a vertical movement of the attracting mass and always checked by a very sensitive tiltmeter. The mass attraction input to the accelerometer was a sine wave with the amplitude of $23 \times 10^{-9}$ $g$. The response of the accelerometer to this acceleration input by mass attraction was obtained by computer data reduction. The results of the experiments agree with the scale factor of the accelerometer for higher acceleration inputs. Application of the mass attraction principle as a calibration method of accelerometers for very low accelerations in orbit is proposed.**


## Nomenclature

$a$ = acceleration of the proof mass along the input axis
$A$ = accelerometer data
$d$ = distance between center of proof mass $m$ and surface of attracting mass $M$
$g$ = Earth gravity (981 cm/sec²)
$I$ = measurement number
$k$ = edge of lead cube
$K$ = harmonic number
$m$ = proof mass of the accelerometer
$M$ = attracting mass
$N$ = number of data
$r$ = radius of a sphere
$R$ = distance between two mass points
$xyz$ = coordinate system fixed to center of proof mass with $x$ axis along the input axis of the accelerometer
$X,Y,Z$ = position of the attracting mass in the $xyz$ system
$\gamma$ = universal gravitational constant ($6.67 \times 10^{-8}$ cm³ g$^{-1}$ sec$^{-2}$)
$\mu g$ = $10^{-6}$ $g$
$a_I$ = acceleration of the proof mass during measurement number $I$
$a_o$ = amplitude of the sinusoidal acceleration


Presented as Paper 70-1030 at the AIAA Guidance, Control and Flight Mechanics Conference, Santa Barbara, Calif., August 17–19, 1970; submitted September 30, 1970; revision received January 15, 1971. This research was accomplished at the Astrionics Laboratory in the George C. Marshall Space Flight Center while the author held a National Research Council Postdoctoral Resident Research Associateship supported by NASA. Thanks are given to B. Walls and G. B. Doane of the Astrionics Laboratory for assistance and support.



* Division Chief, Inertial Techniques and Attitude Simulation, Institut fuer Dynamik der Flugsysteme. Member AIAA.